

## Hydrodynamic and Spectral Simulations of HMXB Winds

Christopher W. MAUCHE<sup>1,\*</sup>, Duane A. LIEHAHL<sup>1,\*\*</sup>, Shizuka AKIYAMA<sup>1,\*\*\*</sup>, and  
Tomek PLEWA<sup>2,†</sup>

<sup>1</sup>*Lawrence Livermore National Laboratory, Livermore, CA 94550, USA*

<sup>2</sup>*University of Chicago, 5640 South Ellis Avenue, RI-475, Chicago, IL 60615, USA*

We describe preliminary results of a global model of the radiatively-driven photoionized wind and accretion flow of the high-mass X-ray binary Vela X-1. The full model combines FLASH hydrodynamic calculations, XSTAR photoionization calculations, HULLAC atomic data, and Monte Carlo radiation transport. We present maps of the density, temperature, velocity, and ionization parameter from a FLASH two-dimensional time-dependent simulation of Vela X-1, as well as maps of the emissivity distributions of the X-ray emission lines.

### §1. Introduction

As described by Castor, Abbott, and Klein (hereafter CAK),<sup>1)</sup> mass loss in the form of a high velocity wind is driven from the surface of an OB star by radiation pressure on a multitude of resonance transitions of intermediate charge states of cosmically abundant elements. The wind is characterized by a mass-loss rate  $\dot{M} \sim 10^{-6}$ – $10^{-5} M_{\odot} \text{ yr}^{-1}$  and a velocity profile  $V(R) \sim V_{\infty}(1 - R_{\text{OB}}/R)^{\beta}$ , where  $\beta \approx \frac{1}{2}$ , the terminal velocity  $V_{\infty} \sim 3 V_{\text{esc}} = 3(2GM_{\text{OB}}/R_{\text{OB}})^{1/2} \sim 1500 \text{ km s}^{-1}$ ,  $R$  is the distance from the OB star, and  $M_{\text{OB}}$  and  $R_{\text{OB}}$  are respectively the mass and radius of the OB star. In a detached high-mass X-ray binary (HMXB), a compact object, typically a neutron star, captures a fraction  $f \sim \pi R_{\text{BH}}^2/4\pi a^2$  of the OB star wind, where  $a$  is the binary separation,  $R_{\text{BH}} = 2GM_{\text{NS}}/[V(a)^2 + c_s^2]$  is the Bondi-Hoyle radius,  $c_s \sim 10(T/10^4)^{1/2} \text{ km s}^{-1}$  is the sound speed, and  $T$  is the wind temperature. Accretion of this material onto the neutron star powers an X-ray luminosity  $L_X \sim f\dot{M}M_{\text{NS}}/R_{\text{NS}} \sim 10^{36}$ – $10^{37} \text{ erg s}^{-1}$ , where  $M_{\text{NS}}$  and  $R_{\text{NS}}$  are respectively the mass and radius of the neutron star. The resulting X-ray flux photoionizes the wind and reduces its ability to be radiatively driven, both because the higher ionization state of the plasma results in a reduction in the number of resonance transitions, and because the energy of the transitions shifts to shorter wavelengths where the overlap with the stellar continuum is lower. To first order, the lower radiative driving results in a reduced wind velocity near the neutron star  $V(a)$ , which increases the Bondi-Hoyle radius  $R_{\text{BH}}$ , which increases the accretion efficiency  $f$ , which increases the X-ray luminosity  $L_X$ . In this way, the X-ray emission of HMXBs is the result of a complex interplay between the radiative driving of the wind of the OB star and the photoionization of the wind by the neutron star.

Known since the early days of X-ray astronomy, HMXBs have been extensively

---

<sup>\*</sup>) E-mail: mauche@cygnus.llnl.gov

<sup>\*\*</sup>) E-mail: liedahl1@llnl.gov

<sup>\*\*\*</sup>) E-mail: shizuka@llnl.gov

<sup>†</sup>) E-Mail: tomek@uchicago.edu

studied observationally, theoretically,<sup>2)–4)</sup> and computationally.<sup>5)–8)</sup> They are excellent targets for X-ray spectroscopic observations because the large covering fraction of the wind and the moderate X-ray luminosities result in large volumes of photoionized plasma that produce strong recombination lines and narrow radiative recombination continua of H- and He-like ions, as well as fluorescent lines from lower charge states.

## §2. Vela X-1

Vela X-1 is the prototypical detached HMXB, having been studied extensively in nearly every waveband, particularly in X-rays, since its discovery as an X-ray source during a rocket flight four decades ago. It consists of a B0.5 Ib supergiant and a magnetic neutron star in an 8.964-day orbit. From an X-ray spectroscopic point of view, Vela X-1 distinguished itself in 1994 when Nagase et al.,<sup>9)</sup> using *ASCA* SIS data, showed that, in addition to the well-known 6.4 keV emission line, the eclipse X-ray spectrum is dominated by recombination lines and continua of H- and He-like Ne, Mg, Si, S, Ar, and Fe. These data were subsequently modeled in detail by Sako et al.,<sup>10)</sup> using a kinematic model in which the photoionized wind was characterized by the ionization parameter  $\xi \equiv L_X/nr^2$ , where  $r$  is the distance from the neutron star and  $n$  is the number density, given by the mass-loss rate and velocity law of an undisturbed CAK wind. Vela X-1 was subsequently observed with the *Chandra* HETG in 2000 for 30 ks in eclipse<sup>11)</sup> and in 2001 for 85, 30, and 30 ks in eclipse and at binary phases 0.25 and 0.5, respectively.<sup>12), 13)</sup> Watanabe et al.,<sup>13)</sup> using very similar assumptions as Sako et al. and a Monte Carlo radiation transfer code, produced a global model of Vela X-1 that simultaneously fit the HETG spectra from the three binary phases with a wind mass-loss rate  $\dot{M} \approx 2 \times 10^{-6} M_\odot \text{ yr}^{-1}$  and terminal velocity  $V_\infty = 1100 \text{ km s}^{-1}$ . One of the failures of this model was the velocity shifts of the emission lines between eclipse and phase 0.5, which were observed to be  $\Delta V \approx 400\text{--}500 \text{ km s}^{-1}$ , while the model simulations predicted  $\Delta V \sim 1000 \text{ km s}^{-1}$ . In order to resolve this discrepancy, Watanabe et al. performed a 1D calculation to estimate the wind velocity profile along the line of centers between the two stars, accounting, in an approximate way, for the reduction of the radiative driving due to photoionization. They found that the velocity of the wind near the neutron star is lower by a factor of 2–3 relative to an undisturbed CAK wind, which was sufficient to explain the observations. However, these results were not fed back into their global model to determine the effect on the X-ray spectra.

## §3. Hydrodynamic Simulations

To make additional progress in our understanding of the wind and accretion flow of Vela X-1 in particular and HMXBs in general — to bridge the gap between the detailed hydrodynamic models of Blondin et al. and the simple kinetic-spectral models of Sako et al. and Watanabe et al. — we have undertaken a project to develop improved models of radiatively-driven photoionized accretion flows, with the goal of producing synthetic X-ray spectral models that possess a level of detail commensurate with the grating spectra returned by *Chandra* and *XMM-Newton*.

This project combines (1) XSTAR<sup>14)</sup> photoionization calculations, (2) HUL-

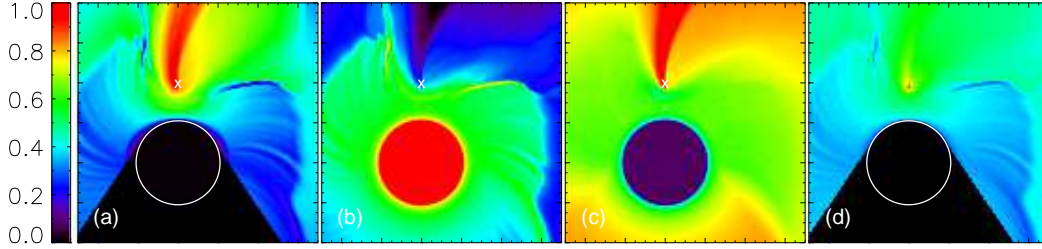


Fig. 1. Color-coded maps of (a)  $\log T(\text{K}) = [4.4, 8.3]$ , (b)  $\log n(\text{cm}^{-3}) = [7.4, 10.8]$ , (c)  $\log V(\text{km s}^{-1}) = [1.3, 3.5]$ , and (d)  $\log \xi(\text{erg cm s}^{-1}) = [1.1, 7.7]$  in the orbital plane of Vela X-1. The positions of the OB star and neutron star are shown by the circle and the “x,” respectively. The horizontal axis  $x = [-5, 7] \times 10^{12}$  cm, and the vertical axis  $y = [-4, 8] \times 10^{12}$  cm.

LAC<sup>15</sup>) emission models appropriate to X-ray photoionized plasmas, (3) improved models of the radiative driving of the photoionized wind, (4) FLASH<sup>16</sup>) three-dimensional time-dependent adaptive-mesh hydrodynamics calculations, and (5) a Monte Carlo radiation transport code.<sup>17</sup>) Radiative driving of the wind is accounted for via the force multiplier formalism,<sup>1)</sup> accounting for X-ray photoionization and non-LTE population kinetics using HULLAC atomic data for  $2 \times 10^6$  lines of 35,000 energy levels of 166 ions of the 13 most cosmically abundant elements. In addition to the usual hydrodynamic quantities, the FLASH calculations account for (a) the gravity of the OB star and neutron star, (b) Coriolis and centrifugal forces, (c) radiative driving of the wind as a function of the local ionization parameter, temperature, and optical depth, (d) photoionization and Compton heating of the irradiated wind, and (e) radiative cooling of the irradiated wind and the “shadow wind” behind the OB star. To demonstrate typical results of our simulations, we show in Fig. 1 color-coded maps of the log of the (a) temperature, (b) density, (c) velocity, and (d) ionization parameter of a FLASH simulation with parameters appropriate to Vela X-1. This is a 2D simulation in the binary orbital plane, has a resolution of  $\Delta l = 9.4 \times 10^{10}$  cm, and, at the time step shown ( $t = 100$  ks), the relatively slow ( $V \approx 400 \text{ km s}^{-1}$ \*) irradiated wind has reached just  $\sim 2$  stellar radii from the stellar surface. The various panels show (1) the effect of the Coriolis and centrifugal forces, which cause the flow to curve clockwise, (2) the cool, fast wind behind the OB star, (3) the hot, slow irradiated wind, (4) the hot, low density, high velocity flow downstream of the neutron star, and (5) the bow shock and two flanking shocks formed where the irradiated wind collides with the hot disturbed flow in front and downstream of the neutron star.

Given these maps, it is straightforward to determine where in the binary the X-ray emission originates. To demonstrate this, we show in Fig. 2 color-coded maps of the log of the emissivity of (a) Si XIV Ly $\alpha$ , (b) Si XIII He $\alpha$ , (c) Fe XXVI Ly $\alpha$ , and (d) Fe XXV He $\alpha$ . The gross properties of these maps agree with Fig. 24 of Watanabe et al., but they are now (1) quantitative rather than qualitative and (2) specific to individual transitions of individual ions. The maps also capture features that otherwise would not have been supposed, such as the excess emission in the H-

\*) Note that this velocity reproduces the value that Watanabe et al. found was needed to match the velocity of the emission lines in the *Chandra* HETG spectra of Vela X-1.

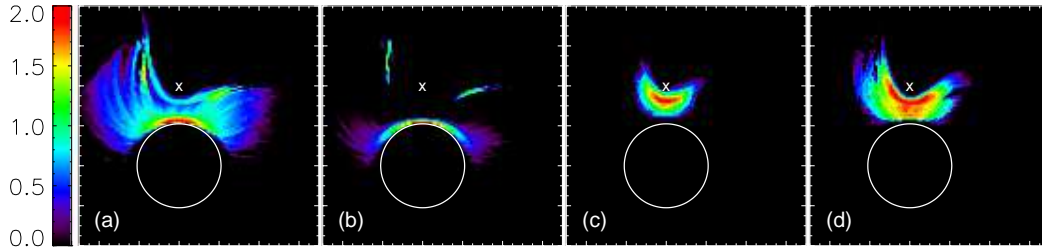


Fig. 2. Color-coded maps of the log of the X-ray emissivity of (a) Si XIV Ly $\alpha$ , (b) Si XIII He $\alpha$ , (c) Fe XXVI Ly $\alpha$ , and (d) Fe XXV He $\alpha$ . In each case, two orders of magnitude are plotted.

and He-like Si lines downstream of the flanking shocks. Combining these maps with the velocity map (Fig. 1c), these models make very specific predictions about (1) the intensity of the emission features, (2) where the emission features originate, and (3) their velocity widths and amplitudes as a function of binary phase.

The next step in our modeling effort is to feed the output of the FLASH simulations into the Monte Carlo radiation transfer code, to determine how the spatial and spectral properties of the X-ray emission features are modified by Compton scattering, photoabsorption followed by radiative cascades, and line scattering. This work is underway.

### Acknowledgements

This work was performed under the auspices of the U.S. Department of Energy by University of California, Lawrence Livermore National Laboratory under Contract W-7405-Eng-48. T. Plewa's contribution to this work was supported in part by the U.S. Department of Energy under Grant No. B523820 to the Center for Astrophysical Thermonuclear Flashes at the University of Chicago.

### References

- 1) J. I. Castor, D. C. Abbott, and R. I. Klein, *Ap.J.* **195** (1975), 157, CAK.
- 2) S. Hatchett and R. McCray, *Ap.J.* **211** (1977), 552.
- 3) R. McCray, T. R. Kallman, J. I. Castor, and G. L. Olson, *Ap.J.* **282** (1984), 245.
- 4) I. R. Stevens and T. R. Kallman, *Ap.J.* **365** (1990), 321.
- 5) J. M. Blondin, T. R. Kallman, B. A. Fryxell, and R. E. Taam, *Ap.J.* **356** (1990), 591.
- 6) J. M. Blondin, I. R. Stevens, and T. R. Kallman, *Ap.J.* **371** (1991), 684.
- 7) J. M. Blondin, *Ap.J.* **435** (1994), 756.
- 8) J. M. Blondin and J. W. Woo, *Ap.J.* **445** (1995), 889.
- 9) F. Nagase, G. Zylstra, T. Sonobe, T. Kotani, H. Inoue, and J. Woo, *Ap.J.* **436** (1994), L1.
- 10) M. Sako, D. A. Liedahl, S. M. Kahn, and F. Paerels, *Ap.J.* **525** (1999), 921.
- 11) N. S. Schulz, C. R. Canizares, J. C. Lee, and M. Sako, *Ap.J.* **564** (2002), L21.
- 12) G. Goldstein, D. P. Huenemoerder, and D. Blank, *A.J.* **127** (2004), 2310.
- 13) S. Watanabe, et al., *Ap.J.* **651** (2006), 421.
- 14) T. Kallman and M. Bautista, *Ap.J.S.* **133** (2001), 221
- 15) A. Bar-Shalom, M. Klapisch, and J. Oreg, *Phys. Rev.* **A38** (1988), 1773
- 16) B. Fryxell, et al., *Ap.J.S.* **131** (2000), 273.
- 17) C. W. Mauche, D. A. Liedahl, B. F. Mathiesen, M. A. Jimenez-Garate, and J. C. Raymond, *Ap.J.* **606** (2004), 168.